AIP | The Journal of Chemical Physics

Orthogonality of embedded wave functions for different states in frozen-density embedding theory

Alexander Zech, Francesco Aquilante, and Tomasz A. Wesolowski

Citation: The Journal of Chemical Physics **143**, 164106 (2015); doi: 10.1063/1.4933372
View online: http://dx.doi.org/10.1063/1.4933372
View Table of Contents: http://scitation.aip.org/content/aip/journal/jcp/143/16?ver=pdfcov
Published by the AIP Publishing

Orthogonality of embedded wave functions for different states in frozen-density embedding theory

Alexander Zech,[1] Francesco Aquilante,[2] and Tomasz A. Wesolowski[1]
[1]*Département de Chimie Physique, Université de Genève, 30 quai Ernest-Ansermet, CH-1211 Genève 4, Switzerland*
[2]*Dipartimento di Chimica "G. Ciamician," Università di Bologna, Via Selmi 2, IT-40126 Bologna, Italy*

(Received 15 July 2015; accepted 6 October 2015; published online 26 October 2015)

Other than lowest-energy stationary embedded wave functions obtained in Frozen-Density Embedding Theory (FDET) [T. A. Wesolowski, Phys. Rev. A **77**, 012504 (2008)] can be associated with electronic excited states but they can be mutually non-orthogonal. Although this does not violate any physical principles — embedded wave functions are only auxiliary objects used to obtain stationary densities — working with orthogonal functions has many practical advantages. In the present work, we show numerically that excitation energies obtained using conventional FDET calculations (allowing for non-orthogonality) can be obtained using embedded wave functions which are strictly orthogonal. The used method preserves the mathematical structure of FDET and self-consistency between energy, embedded wave function, and the embedding potential (they are connected through the Euler-Lagrange equations). The orthogonality is built-in through the linearization in the embedded density of the relevant components of the total energy functional. Moreover, we show formally that the differences between the expectation values of the embedded Hamiltonian are equal to the excitation energies, which is the exact result within linearized FDET. Linearized FDET is shown to be a robust approximation for a large class of reference densities. © *2015 AIP Publishing LLC*. [http://dx.doi.org/10.1063/1.4933372]

I. INTRODUCTION

In multi-scale simulations based on Frozen-Density Embedding Theory (FDET),[1–3] all information about the environment of a subsystem, which is described using quantum mechanical descriptors, is contained in the positive and negative charge densities. In particular, the electron density $\rho_B(\vec{r})$ describes the electronic state of the environment. The present work concerns the variant of FDET in which an interacting wave function (Ψ_A) is used to describe the electronic state of the embedded species.[2] Other variants of FDET use for this purpose: a reference system of noninteracting electrons[1] and one-particle spinless reduced density matrices.[3] In the working equations of FDET, $\rho_B(\vec{r})$ is a given function, i.e., frozen, and the optimal embedded wave function Ψ_A^o is obtained as the lowest-energy solution of the Euler-Lagrange equation. Following the Levy-Perdew theorem,[4] other than the lowest energy solutions of the Euler-Lagrange equation of FDET can be associated with excited states as noticed by Khait and Hoffmann.[5] Without further approximations concerning the FDET embedding potential, FDET based methods feature a qualitative difference from most of other embedding methods used in practice — the FDET embedding potential depends on the embedded density ($\rho_A(\vec{r})$). This leads to the following practical consequences.

(A) Additional contribution to the response kernel in the linear-response time-dependent DFT calculations of excited states.[6]

(B) Expectation value of the embedding potential cannot be interpreted as the corresponding contribution to the energy of the interaction between the embedded species and its environment.

(C) Different stationary embedded wave functions obtained from variational calculations are not orthogonal,

$$\langle \Psi_A^I | \Psi_A^J \rangle \neq \delta_{IJ}. \tag{1}$$

The present work concerns mainly the third issue. In Ref. 7, we proposed the approximate formulation of FDET in which the orthogonality of embedded wave functions is assured by construction. We will refer to this formulation as *linearized FDET*. In the present work, we analyze numerically the relation between the results obtained using the *linearized FDET* and conventional FDET calculations.

The interest in using the density-dependent embedding potentials in combinations with correlated methods of quantum chemistry has been systematically growing (see the recent review by Bendavid and Carter,[8] our recent review,[9] or representative publications from various research groups in Refs. 5 and 10–16). Such methods follow either the energy-error cancellation scheme proposed by Carter *et al.*[17,18] or the formal framework of FDET.[2] The error cancellation scheme belongs to the larger group of methods called collectively in the literature as the *ONIOM strategy* (the term coined in the works by Morokuma and collaborators[19]); the independent variables describing the whole system are the electron density of the whole system ($\rho_{total}(\vec{r})$) and the embedded wave function (Ψ_A). $\rho_{total}(\vec{r})$ is obtained from some lower-quality quantum

mechanical calculations. In FDET, on the other hand, the independent variables are $\rho_B(\vec{r})$ and the embedded wave function Ψ_A. The key difference between FDET and the ONIOM type of methods is the choice of independent variables for describing the state of the whole system. An explicit quantum mechanical descriptor for the system as the whole (such as an approximated wave function) is not constructed in the formal framework of FDET at all.

In either ONIOM or FDET type of methods, the embedding potential depends on the embedded density $\rho_A(\vec{r})$, which is constructed from the embedded wave function Ψ_A. The possible drawbacks due to the ρ_A-dependence of the embedding potential and the resulting non-orthogonality concern, therefore, both type of methods. In view of a large number of additional approximations used in such methods, we refer the reader to our recent comprehensive review[9] on FDET based multi-level simulation methods or the relevant sections of other reviews.[20–22,8] We underline only the fact that in most of density-based embedding methods (either ONIOM and FDET type), an additional approximation is made by making the embedding potential ρ_A-independent. It is usually done by evaluating the embedding potential at some fixed density $\rho_A^{ref}(\vec{r})$, which is not equal to the density corresponding to the optimal embedded wave function

$$\rho_A^{ref}(\vec{r}) \neq \rho_A^I(\vec{r}) = \left\langle \Psi_A^I \middle| \sum_{i=1}^{N_A} \delta(\vec{r} - \vec{r}_i) \middle| \Psi_A^I \right\rangle \qquad (2)$$

in the investigated state.[18,12,23,14] With a fixed potential density, embedding involves a trivial modification of any method from the toolbox of quantum chemistry (see the recent textbook by Helgaker, Olsen, and Jorgensen,[24] for instance). The embedding potential results in an additional one-electron term in the Hamiltonian. Alternatively, a fixed (i.e., ρ_A-independent) embedding potential can be derived by the inversion technique[25–30] leading to similar advantages.

Using a fixed embedding potential leads, however, to the inconsistency between the energy and embedded wave function. The stationary state Ψ_A^I is obtained using the embedding potential, which is not evaluated at the corresponding density $\rho_A^I(\vec{r})$ but at some other density. To our knowledge, the only numerical studies taking into account ρ_A-dependency embedding potentials within the FDET framework have been conducted by Neugebauer and collaborators.[11,10,16] The self-consistency between the embedding potential and the embedded wave function was achieved by means of an iterative procedure consisting of successive updating $\rho_A^{ref}(\vec{r})$ by using $\rho_A(\vec{r})$ from the previous iteration. The procedure was shown to converge quickly in the case of embedding a non-interacting wave function.[31] It was shown to be efficient also in the case of embedding an interacting system[10,16] and is applied also in the present work for performing conventional FDET calculations. In the context of ONIOM methods, this iterative procedure was introduced in Ref. 18. The issue of numerical importance of the orthogonality was not discussed in Refs. 11 and 10, which concerned mainly another effect — the differential polarization of the environment for different electronic states of the embedded species. This effect obviously contributes also to the non-orthogonality. In the FDET terminology, this means ρ_B-dependency. Similar situation concerns the embedding methods taking into account differential response of the environment to the change of the environment: continuum models[32,33] or discrete polarizabilities.[34–36] In the context of FDET, it is worthwhile to notice that division of the total density into the $\rho_A(\vec{r})$ and $\rho_B(\vec{r})$ components is not unique and the same energy and density of the total system can be obtained for different choices for $\rho_B(\vec{r})$ (see discussions in Refs. 20 and 37, analytical examples in Ref. 38, and numerical examples in Ref. 39, for instance). This leads to non-unique definition of polarization of the environment. The relative importance of the ρ_A- and ρ_B-dependency of the embedding potential cannot, therefore, be assessed in a straightforward manner. For this reason, the present work reports the results obtained with the same $\rho_B(\vec{r})$ for each considered electronic state of the embedded species.

More recently, Dresselhaus and Neugebauer reported the numerical results concerning the orthogonality of the embedded wave functions associated with different states obtained using the FDET embedding potential as derived in Ref. 2, i.e., ρ_A-dependent embedding potential.[65] The non-orthogonality in the reported calculations originated also from other factors than the ρ_A-dependence of the FDET embedding potential: ρ_B-dependence of the FDET embedding potential and the use of Complete Active Space Self-Consistent Field (CASSCF) treatment of many electron problem for $\rho_A(\vec{r})$. It was shown that ρ_A-dependency contributes to the overlap between the wave functions associated with different states significantly less than other factors. In the present work, we also report the numerical results of the overlap obtained using a computational protocol aimed directly at estimation of the overlap due to ρ_A-dependence. The excitation energies obtained using such non-orthogonal embedded wave functions are used as a reference for the linearized FDET results.

The principal objective of the present work concerns such computational methods where the embedding potential is fixed, i.e., it is obtained by means of evaluating the FDET functional for this potential not at the actual ρ_A^I but at some other (fixed) density. The embedding calculations of this type are quite common and use various methods to solve quantum-many-body problem for the embedded subsystem combined with an approximated FDET potential.[12,40,23,11,16] Fixing the embedding potential leads to orthogonal embedded wave functions but results in the inconsistency between the used FDET expressions for the energy and the embedding potential. The latter is no more obtained as the functional derivative of the corresponding energy contributions. The consistency can easily be restored without additional computational cost using the method proposed in Ref. 7 (labeled as "method B" there and "linearized FDET" in the present work).

The present work has the following structure. Section II provides the key elements of the conventional formulation of FDET for embedding an interacting wave function, which was given originally in Ref. 2. The linearized version of FDET proposed in Ref. 7 for excited states is given in Section III. We present details of our calculations in Section IV. In Section V, the numerical results obtained in the present study by means of either versions of the FDET are displayed and discussed in Section VI.

II. FROZEN-DENSITY EMBEDDING THEORY

In this section, the key elements and definitions of frozen-density embedding theory are given in their version for embedding a system of interacting electrons as formulated in Ref. 2. Unless indicated by the use of tildes, the definitions are given for the exact formulation, i.e., they hold for the exact functionals. ρ, ρ_A, ρ_B, and Ψ_A denote arguments of the functionals. Specific functions are indicated by means of superscripts.

Frozen-density embedding theory concerns the following constrained search problem in which the number of electrons N_{AB}, the external potential $v_{AB}(\vec{r})$, and some non-negative function $\rho_B(\vec{r})$ is the given quantities:

$$E^{FDET}[\rho_B] = \min_{\substack{\forall \vec{r}\ \rho(\vec{r}) \geq \rho_B(\vec{r}) \\ \int \rho(\vec{r}) d\vec{r} = N_{AB}}} E^{HK}_{v_{AB}}[\rho] = E^{HK}_{v_{AB}}[\rho^{FDET}_{AB}]. \quad (3)$$

If the trial densities in the above search $\rho(\vec{r})$ are represented as

$$\rho(\vec{r}) = \rho_B(\vec{r}) + \left\langle \Psi_A \left| \sum_{i=1}^{N_A} \delta(\vec{r} - \vec{r}_i) \right| \Psi_A \right\rangle, \quad (4)$$

where Ψ_A has the form of a N_A-electron function, the condition $\forall \vec{r}\ \rho(\vec{r}) \geq \rho_B(\vec{r})$ is automatically satisfied.

Expressing the total energy as a functional $E^{EWF}_{AB}[\Psi_A, \rho_B]$, which depends explicitly on Ψ_A and $\rho_B(\vec{r})$, makes it possible to use the Euler-Lagrange equation in order to find stationary many-electron wave functions,

$$\frac{\delta E^{EWF}_{AB}[\Psi^I_A, \rho_B]}{\delta \Psi^I_A} - \lambda^I \Psi^I_A = 0, \quad (5)$$

where λ^I is the Lagrange multiplier associated with the normalization. The index I indicates that the present work concerns not only in the lowest-energy solution but also other stationary states.

The total energy functional denoted as $E^{EWF}_{AB}[\Psi_A, \rho_B]$ reads

$$\begin{aligned} E^{EWF}_{AB}[\Psi_A, \rho_B] &= \langle \Psi_A | \hat{H}_A | \Psi_A \rangle + E^{nad}_{xct}[\rho_A, \rho_B] \\ &+ \int \rho_A(\vec{r}) v_B(\vec{r}) d\vec{r} + \int\int \frac{\rho_A(\vec{r}) \rho_B(\vec{r}')}{|\vec{r} - \vec{r}'|} d\vec{r}' d\vec{r} \\ &+ E^{HK}_{v_B}[\rho_B] + \int \rho_B(\vec{r}) v_A(\vec{r}) d\vec{r}, \end{aligned} \quad (6)$$

where the functional $E^{nad}_{xct}[\rho_A, \rho_B]$ comprises three components,

$$E^{nad}_{xct}[\rho_A, \rho_B] = T^{nad}_s[\rho_A, \rho_B] + E^{nad}_{xc}[\rho_A, \rho_B] + \Delta F^{SC}[\rho_A]. \quad (7)$$

The non-additive bi-functionals $T^{nad}_s[\rho_A, \rho_B]$ and $E^{nad}_{xc}[\rho_A, \rho_B]$, and the functional $\Delta F^{SC}[\rho_A]$ are defined by means of the constrained search procedure (see below in this section).

The necessary condition for Ψ^I_A to satisfy Eq. (5) takes the form resembling the conventional Schrödinger equation for many-electrons,

$$\left(\hat{H}_A + \hat{v}_{emb}\right) \Psi^I_A = \epsilon^I \Psi^I_A, \quad (8)$$

where $\hat{v}_{emb}$ denotes the "*embedding operator*" given in the form of the potential which in turn is uniquely determined by the charge densities $\rho_A(\vec{r})$ and $\rho_B(\vec{r})$ and the fixed potential $v_B(\vec{r})$. The functional for this potential is obtained as the functional derivative of the corresponding terms in the total energy functional (Eq. (6)) and reads

$$\begin{aligned} v_{emb}[\rho_A, \rho_B, v_B](\vec{r}) &= v_B(\vec{r}) + \int \frac{\rho_B(\vec{r}')}{|\vec{r}' - \vec{r}|} d\vec{r}' \\ &+ \frac{\delta E^{nad}_{xct}[\rho_A, \rho_B]}{\delta \rho_A(\vec{r})}. \end{aligned} \quad (9)$$

The FDET embedding potential comprises the classical electrostatic components (the first two terms in the RHS of Eq. (9), which do not depend on ρ_A) and the terms which are defined as functional derivatives of the density functionals: $T^{nad}_s[\rho_A, \rho_B]$, $E^{nad}_{xc}[\rho_A, \rho_B]$, and $\Delta F^{SC}[\rho_A]$. The latter are, therefore, also the functionals of ρ_A and ρ_B.

The bi-functional $T^{nad}_s[\rho_A, \rho_B]$ is defined using the constrained search procedure[41] for the density functional of the kinetic energy in the reference system of non-interacting electrons $T_s[\rho]$,

$$\begin{aligned} T^{nad}_s[\rho_A, \rho_B] &= \min_{\Psi_s \to \rho_A + \rho_B} \langle \Psi_s | \hat{T} | \Psi_s \rangle \\ &- \min_{\Psi_s \to \rho_A} \langle \Psi_s | \hat{T} | \Psi_s \rangle - \min_{\Psi_s \to \rho_B} \langle \Psi_s | \hat{T} | \Psi_s \rangle \\ &= \left\langle \Psi^{AB(opt)}_s[\rho_A + \rho_B] \left| \hat{T} \right| \Psi^{AB(opt)}_s[\rho_A + \rho_B] \right\rangle \\ &- \left\langle \Psi^{A(opt)}_s[\rho_A] \left| \hat{T} \right| \Psi^{A(opt)}_s[\rho_A] \right\rangle \\ &- \left\langle \Psi^{B(opt)}_s[\rho_B] \left| \hat{T} \right| \Psi^{B(opt)}_s[\rho_B] \right\rangle. \end{aligned} \quad (10)$$

The non-additive exchange-correlation bi-functional $E^{nad}_{xc}[\rho_A, \rho_B] = E_{xc}[\rho_A + \rho_B] - E_{xc}[\rho_A] - E_{xc}[\rho_B]$ is defined in a similar way starting from the well-known exchange-correlation functional ($E_{xc}[\rho]$) of the Kohn-Sham formulation of DFT.[42]

Concerning the functional $\Delta F^{SC(WFT)}[\rho]$, its definition depends on what is used as $\hat{H}_A$ and on the search domain. In the case of interacting Hamiltonian, it reads

$$\begin{aligned} \Delta F^{SC(WFT)}[\rho_A] &= \min_{\Psi_A \longrightarrow \rho_A} \left\langle \Psi_A \left| \hat{T}_{2N_A} + \hat{V}^{ee}_{2N_A} \right| \Psi_A \right\rangle \\ &- \min_{\Psi^{WF}_A \longrightarrow \rho_A} \left\langle \Psi^{WF}_A \left| \hat{T}_{2N_A} + \hat{V}^{ee}_{2N_A} \right| \Psi^{WF}_A \right\rangle, \end{aligned} \quad (11)$$

where Ψ^{WF}_A indicates a trial function used in the search procedure of the form admissible in the used wave function based method, whereas Ψ_A is a trial wave function from the wider class of functions comprising all v-representable densities.[41,43] Ψ^{WF}_A can take any form used in variational-principle conventional wave function methods of quantum chemistry (see the classic textbook by Szabo and Ostlund[44] or a more recent one by Helgaker, Olsen, and Jorgensen,[24] for instance) starting from as simple as a single determinant (Ψ^{SD}_A) in the Hartree-Fock method, through the forms in *CASSCF* or truncated configuration interaction *(CI)* methods, until the one in full *CI* calculations.

$\Delta F^{SC(WFT)}[\rho_A]$ is non-positive and it is bound from below by

$$\begin{aligned} \Delta F^{SC(SD)}[\rho_A] &= \min_{\Psi_A \longrightarrow \rho_A} \left\langle \Psi_A \left| \hat{T}_{2N_A} + \hat{V}^{ee}_{2N_A} \right| \Psi_A \right\rangle \\ &- \min_{\Psi^{SD}_A \longrightarrow \rho_A} \left\langle \Psi^{SD}_A \left| \hat{T}_{2N_A} + \hat{V}^{ee}_{2N_A} \right| \Psi^{SD}_A \right\rangle. \end{aligned} \quad (12)$$

The zero value is reached only in the limit of the embedded wave function of the full *CI* form. For truncated *CI* forms of

the embedded wave function, the numerical values of this functional lie between the two limits. In all simulations based on FDET, the density functionals $T_s^{nad}[\rho_A,\rho_B]$ and $E_{xc}^{nad}[\rho_A,\rho_B]$ are approximated and these approximations determine the overall quality of the obtained results. Except for model studies,[45] in all such applications, the functional $\Delta F^{SC(WFT)}[\rho_A]$ is neglected.

Concerning the excited states, if the Euler-Lagrange equation for the embedded wave function, i.e., Eq. (8), has several solutions, the other than lowest energy solutions can be associated with excited states on the virtue of the Levy-Perdew theorem.[4] Such interpretation of these solutions was first pointed out by Khait and Hoffman.[5]

In multi-scale simulation methods based on FDET, the exact density functionals in Eq. (7) $T_s^{nad}[\rho_A,\rho_B]$, $E_{xc}^{nad}[\rho_A,\rho_B]$, and $\Delta F^{SC(WFT)}[\rho_A]$ are replaced by their approximate counterparts: $\tilde{T}_s^{nad}[\rho_A,\rho_B]$, $\tilde{E}_{xc}^{nad}[\rho_A,\rho_B]$, and $\Delta\tilde{F}^{SC(WFT)}[\rho_A]$.

In such a case, the embedded electron density is obtained from Euler-Lagrange equations,

$$\frac{\delta\tilde{E}_{AB}^{EWF}[\Psi_A^I,\rho_B]}{\delta\Psi_A^I}-\lambda^I\Psi_A^I=0, \tag{13}$$

where the exact energy expression (Eq. (6)) is replaced by an approximated functional,

$$\begin{aligned}\tilde{E}_{AB}^{EWF}[\Psi_A,\rho_B]&=\langle\Psi_A|\hat{H}_A|\Psi_A\rangle+\tilde{E}_{xct}^{nad}[\rho_A,\rho_B]\\&+\int\rho_A(\vec{r})v_B(\vec{r})d\vec{r}+\int\int\frac{\rho_A(\vec{r})\rho_B(\vec{r}')}{|\vec{r}-\vec{r}'|}d\vec{r}'d\vec{r}\\&+E_{v_B}^{HK}[\rho_B]+\int\rho_B(\vec{r})v_A(\vec{r})d\vec{r}.\end{aligned} \tag{14}$$

The above compact form of the Euler-Lagrange equation for the embedded wave function covers various variational principle based methods from the toolbox of computational chemistry.

III. LINEARIZED FDET

The *linearized FDET* was proposed in Ref. 7 and the present section provides a summary of the key equations. The tilde in the equations given in the present section (such as in $\tilde{E}_{xct}^{nad}[\rho_A,\rho_B]$, for instance) indicates that the respective functional is approximated.

Linearization consists of approximating the functional $E_{xct}^{nad}[\rho_A,\rho_B]$ by a functional which is linear in ρ_A and using such an approximation in the FDET equations (Eqs. (6), (5), and (9)). Starting from some approximated functional $\tilde{E}_{xct}[\rho_A,\rho_B]$, a new — linearized — approximation is constructed as

$$\tilde{E}_{xct}^{nad}[\rho_A,\rho_B]\approx\tilde{E}_{xct}^{nad(lin)}\left[\rho_A,\rho_B,\rho_A^{ref}\right]=\tilde{E}_{xct}^{nad}\left[\rho_A^{ref},\rho_B\right]+\int\left(\rho_A(\vec{r})-\rho_A^{ref}(\vec{r})\right)\left.\frac{\delta\tilde{E}_{xct}^{nad}[\rho_A,\rho_B]}{\delta\rho_A(\vec{r})}\right|_{\rho_A=\rho_A^{ref}}d\vec{r}, \tag{15}$$

where $\rho_A^{ref}(\vec{r})$ is some density which does not differ significantly from the stationary density of the embedded species.

Insertion of the linearized approximation for $E_{xct}^{nad}[\rho_A,\rho_B]$ given in Eq. (15) into the FDET energy expression (Eq. (6)) and evaluation of the corresponding functional derivative with respect to ρ_A lead to

$$\begin{aligned}\tilde{v}_{emb}^{lin}[\rho_A,\rho_B,v_B,\rho_A^{ref}](\vec{r})&=v_B(\vec{r})+\int\frac{\rho_B(\vec{r}')}{|\vec{r}'-\vec{r}|}d\vec{r}'+\left.\frac{\delta\tilde{E}_{xct}^{nad(lin)}\left[\rho_A,\rho_B,\rho_A^{ref}\right]}{\delta\rho_A}\right|_{\rho_A=\rho_A^{ref}}\\&=v_B(\vec{r})+\int\frac{\rho_B(\vec{r}')}{|\vec{r}'-\vec{r}|}d\vec{r}'+\left.\frac{\delta\tilde{E}_{xct}^{nad}\left[\rho_A,\rho_B,\rho_A^{ref}\right]}{\delta\rho_A}\right|_{\rho_A=\rho_A^{ref}}\\&=\tilde{v}_{emb}[\rho_A^{ref},\rho_B,v_B](\vec{r}),\end{aligned} \tag{16}$$

which is ρ_A-independent. It is just the potential obtained using the original (non-linear) approximated functional $\tilde{E}_{xct}^{nad}[\rho_A,\rho_B]$ evaluated not at the stationary density corresponding to a given electronic state of the embedded species (Ψ_A^I) but at $\rho_A(\vec{r})=\rho_A^{ref}(\vec{r})$.

The linearization can be made with any approximation for $E_{xct}^{nad}[\rho_A,\rho_B]$ and results in a great simplification of the FDET equations. In particular, the embedding potential becomes ρ_A-independent which assures orthogonality of all stationary embedded wave functions Ψ_A^I by construction.

From the point of view of solving a many electron problem, the linearized embedding potential is just a fixed potential which will be denoted here as just $\tilde{v}_{emb}^{lin}(\vec{r})$. Eq. (8) then becomes

$$\left(\hat{H}_A+\hat{v}_{emb}^{lin}\right)\Psi_A^I=\epsilon^I\Psi_A^I, \tag{17}$$

where

$$\hat{v}_{emb}^{lin}=\sum_{i=1}^{N_A}\tilde{v}_{emb}^{lin}(\vec{r})\delta(\vec{r}-\vec{r}_i). \tag{18}$$

If Eq. (17) is solved by means of any method from the toolbox of quantum chemistry, the use of the potential given in Eq. (16) represents a trivial modification — change of the one-electron component of the Hamiltonian $\hat{H}_A$.

In principle, various choices can be made for $\rho_A^{ref}(\vec{r})$. The smaller is the difference $\Delta\rho_A^I(\vec{r})=\rho_A^I(\vec{r})-\rho_A^{ref}(\vec{r})$, the

less significant are the truncated terms in the expansion of $E_{xct}^{nad}[\rho_A, \rho_B]$ about $\rho_A^{ref}(\vec{r})$.

As the *linearized FDET*, we understand the formal framework scheme in which Eq. (16) is used as the embedding potential in Eq. (8) and the non-additive energy components in the total energy $T_s^{nad}[\rho_A, \rho_B]$ and $E_{xc}^{nad}[\rho_A, \rho_B]$ are evaluated by means of Eq. (15).

For further analysis, it is convenient to write the expression for the total electronic energy in *Linearized FDET* as

$$\begin{aligned} E_{AB}^{LinFDET}[\Psi_A, \rho_B, \rho_A^{ref}] &= \langle \Psi_A | \hat{H}_A | \Psi_A \rangle \\ &+ \int \rho_A(\vec{r}) v_B(\vec{r}) d\vec{r} + \int\int \frac{\rho_A(\vec{r})\rho_B(\vec{r}')}{|\vec{r} - \vec{r}'|} d\vec{r}' d\vec{r} \\ &+ \tilde{E}_{xct}^{nad}[\rho_A^{ref}, \rho_B] + \Delta^{lin}[\rho_A, \rho_A^{ref}, \rho_B] \\ &+ E_{v_B}^{HK}[\rho_B] + \int \rho_B(\vec{r}) v_A(\vec{r}) d\vec{r}, \end{aligned} \tag{19}$$

where

$$\begin{aligned} &\Delta^{lin}[\rho_A, \rho_A^{ref}, \rho_B] \\ &= \int \left(\rho_A(\vec{r}) - \rho_A^{ref}(\vec{r})\right) \left.\frac{\delta \tilde{E}_{xct}^{nad}[\rho_A, \rho_B]}{\delta \rho_A(\vec{r})}\right|_{\rho_A = \rho_A^{ref}} d\vec{r}. \end{aligned} \tag{20}$$

In the above expression, the terms $E_{v_B}^{HK}[\rho_B] + \int \rho_B(\vec{r}) v_A(\vec{r}) d\vec{r}$ do not depend on ρ_A at all. They will not be considered further. The first three terms in the right-hand-side are obviously state-dependent as they change if Ψ_A changes. These terms can be evaluated as expectation values of the corresponding usual operators. The only state-dependent term evaluated by means of an approximated density functional is $\Delta^{lin}[\rho_A, \rho_A^{ref}, \rho_B]$, which is a convenient quantity in assessment of the quality of the used reference density $\rho_A^{ref}(\vec{r})$.

Using the definition of the potential $\hat{v}_{emb}^{lin}$ (Eq. (16)), the total energy expression can be written alternatively as

$$\begin{aligned} E_{AB}^{LinFDET}[\Psi_A, \rho_B, \rho_A^{ref}] &= \langle \Psi_A | \hat{H}_A + \hat{v}_{emb}^{lin} | \Psi_A \rangle + \tilde{E}_{xct}^{nad}[\rho_A^{ref}, \rho_B] - \int \rho_A^{ref}(\vec{r}) \left.\frac{\delta \tilde{E}_{xct}^{nad}[\rho_A, \rho_B]}{\delta \rho_A(\vec{r})}\right|_{\rho_A = \rho_A^{ref}} d\vec{r} \\ &+ E_{v_B}^{HK}[\rho_B] + \int \rho_B(\vec{r}) v_A(\vec{r}) d\vec{r}. \end{aligned} \tag{21}$$

Applying the above formula for evaluating the difference between the energies corresponding to different stationary states of the embedded system (say Ψ_A^K and Ψ_A^L) yields

$$\begin{aligned} \Delta_{KL} &= E_{AB}^{LinFDET}[\Psi_A^K, \rho_B, \rho_A^{ref}] - E_{AB}^{LinFDET}[\Psi_A^L, \rho_B, \rho_A^{ref}] \\ &= \langle \Psi_A^K | \hat{H}_A + \hat{v}_{emb}^{lin} | \Psi_A^K \rangle - \langle \Psi_A^L | \hat{H}_A + \hat{v}_{emb}^{lin} | \Psi_A^L \rangle, \end{aligned} \tag{22}$$

which holds for any approximation to $E_{xct}^{nad}[\rho_A, \rho_B]$ of the form given in Eq. (15). Note that the operator $\hat{v}_{emb}^{lin}$ is *the same* in both terms of the second line of Eq. (22).

Eq. (22) is very useful in practice. It shows that evaluation of only the expectation value $\langle \Psi_A | \hat{H}_A + \hat{v}_{emb}^{lin} | \Psi_A \rangle$ is needed to obtain excitation energies in *linearized FDET*. The absolute value of the energy at each state requires, however, the evaluation of the contribution due to the inhomogeneity of $E_{xct}^{nad}[\rho_A, \rho_B]$ (the two terms in the second line of Eq. (21)). The magnitude of this contribution might depend on the particular case (the overlap between $\rho_A(\vec{r})$ and $\rho_B(\vec{r})$) as well as on the used approximation—$\tilde{E}_{xct}^{nad}[\rho_A, \rho_B]$.

It is worthwhile to notice in Eq. (22) that the errors in the excitation energies in *linearized FDET* depend only on the error in the potential (functional derivative of $E_{xct}^{nad}[\rho_A, \rho_B]$). The state-independent contributions to the total energy functional given in Eq. (21) do not contribute to the energy differences. The situation is similar to that in case of using the FDET embedding potential to obtain excitation energies from the LR-TDDFT framework[46] as proposed in Ref. 6. The direct relation between the embedding potential and the energy differences in *linearized FDET* suggests the bottom-up approach in construction of approximations for $E_{xct}^{nad}[\rho_A, \rho_B]$. Instead of starting from some approximated analytical expression for the functional $\tilde{E}_{xct}^{nad}[\rho_A, \rho_B]$ and using it to obtain the corresponding potential $\frac{\delta \tilde{E}_{xct}^{nad}[\rho_A, \rho_B]}{\delta \rho_A(\vec{r})}$, one should rather start from approximating $\frac{\delta E_{xct}^{nad}[\rho_A, \rho_B]}{\delta \rho_A(\vec{r})}$ because the "parent" functional is not even needed in the evaluation of the excitation energies. The construction of the NDSD (Non-Decomposable using Second Derivatives) approximation for $T_s^{nad}[\rho_A, \rho_B]$[47] is an example of such bottom-up approach. The NDSD potential satisfied one of the conditions for the exact $\frac{\delta T_s^{nad}[\rho_A, \rho_B]}{\delta \rho_A(\vec{r})}$ (its asymptotic behavior far from nucleus given in Ref. 47) at the expense of violating another condition satisfied by $T_s^{nad}[\rho_A, \rho_B]$,

$$T_s^{nad}[\rho_A, \rho_B] = T_s^{nad}[\rho_B, \rho_A]. \tag{23}$$

Eq. (22) shows clearly that respecting exact conditions for the density functional for the embedding potential is more important than the ones for the density functional for the corresponding energy components in the case of *linearized FDET*.

In the Euler-Lagrange equation for the embedded wave function (Eq. (13)), either the FDET expression for the total energy functional or the linearized FDET expression (Eq. (19)) can be applied. Inspection of the two functionals shows clearly that only the latter one, i.e., Eq. (19), leads to the embedding potential which does not depend on the embedded wave function.

IV. NUMERICAL DETAILS

The Euler-Lagrange equation of FDET (Eq. (5)) was solved using the CASSCF methodology. In order to study state-specificity of the embedding potential, only one root was

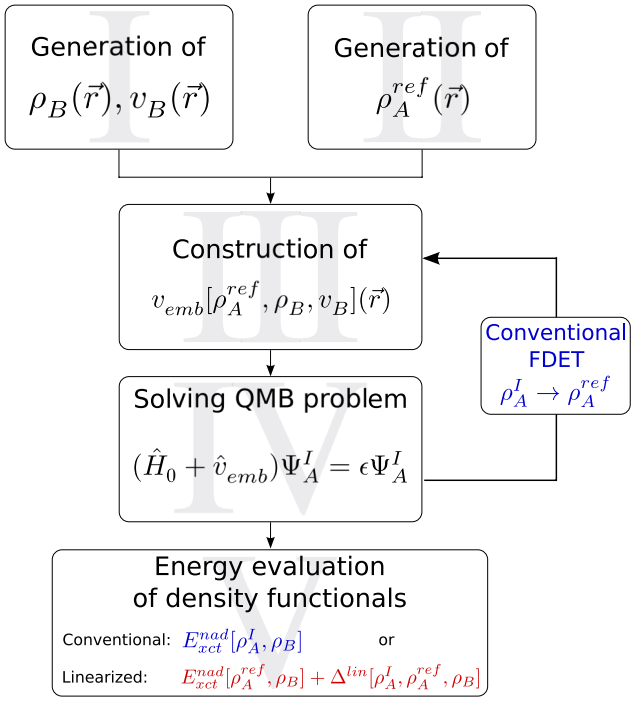

FIG. 1. Procedure of conventional and linearized FDET.

considered at a time by assigning 100% weight to the selected root and orbital optimization was disabled resulting in CAS Configuration Interaction (CASCI). Note that only if variational principle methods are used to solve Eq. (8), the obtained stationary wave functions satisfy Eq. (5). Figure 1 summarizes the FDET protocol used in this study. First, the environment density was generated at the Hartree-Fock level of theory and kept constant throughout the embedding calculations. As for step II, $\rho_A^{ref}(\vec{r})$ was retrieved from a CASCI calculation on the isolated system A, which used orbitals from a preliminary state-averaged CASSCF calculation. In the first iteration of step III and IV, the embedding potential is constructed using the CASCI ground state density of the isolated system A. After solving Eq. (8), the embedding potential is updated with the new embedded density of system A. Steps III and IV were repeated until self-consistency (i.e., change in total energy $<10^{-8}$ Hartree) was achieved. For all tested systems, three macrocycles were needed.

The calculations were performed using a development version of the Molcas quantum chemistry software.[48,49] The cc-pVTZ basis set was used in all FDET calculations except for the bromine model system, where the aug-cc-pVDZ basis set was applied.[50,51] The implementation uses Cholesky-based *ab initio* density fitting[52] to approximate the two-electron integrals: the required auxiliary basis set is not pre-optimized through data-fitting but it is generated through Cholesky decomposition of each atomic sub-block of the integral matrix. Next to the computational advantage compared to conventional integral calculations, this type of density fitting guarantees to a large extent complete error control in the computed energy[53,54] and energy gradients.[55–57] Unless otherwise stated, the threshold for the atomic Cholesky decompositions was set to 10^{-4} a.u. The Thomas-Fermi kinetic energy functional[58,59] and the PBE (Perdew-Burke-Ernzerhof) exchange-correlation functional[60] were employed in the evaluation of $T_s^{nad}[\rho_A, \rho_B]$ and $E_{xc}^{nad}[\rho_A, \rho_B]$, respectively.

V. RESULTS

A. Systems

For this investigation, monohydrates of uracil, a model dipeptide, and bromine were selected. Uracil serves as a common example for local $n \rightarrow \pi^*$ and $\pi \rightarrow \pi^*$ excitations. Three different uracil monohydrates were considered in the embedding calculations, which will be referenced to as **U1**, **U3**, and **U4** from here on.[61] Using three monohydrates on the basis of the same molecule also allowed us to study the behavior of the linearization depending on the position of $\rho_B(\vec{r})$ with respect to the embedded species. In this way, we covered cases with different overlaps of $\rho_A(\vec{r})$ and $\rho_B(\vec{r})$. Since for the uracil monohydrates, changes in $\rho_A(\vec{r})$ occur mainly locally for the investigated excited states; there was also the need for a system where larger changes are observed. For this reason, the model dipeptide depicted in Fig. 3 was chosen as an example for charge-transfer excitations.[62,63] Another category of systems with strong solvent shift is halogen-water clusters. For this study, bromine monohydrate, isomer **1a** from Ref. 64, was selected (see Fig. 4). This monohydrate shows significant changes in the density upon excitation of the bromine molecule.[14] It is also a good example for a system in which polarization is a prominent feature.[64] In the following, we will refer to

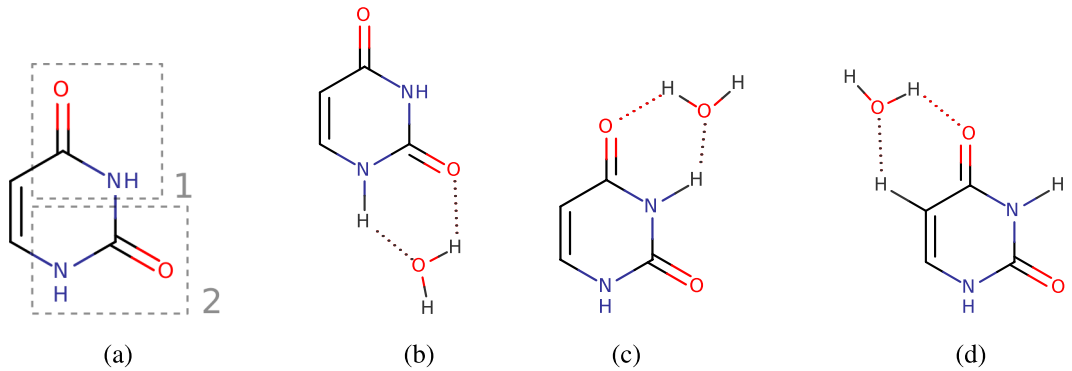

FIG. 2. Studied uracil-H_2O complexes. (a) Convention used in the text to distinguish the peptide units. (b) U1. (c) U3. (d) U4.

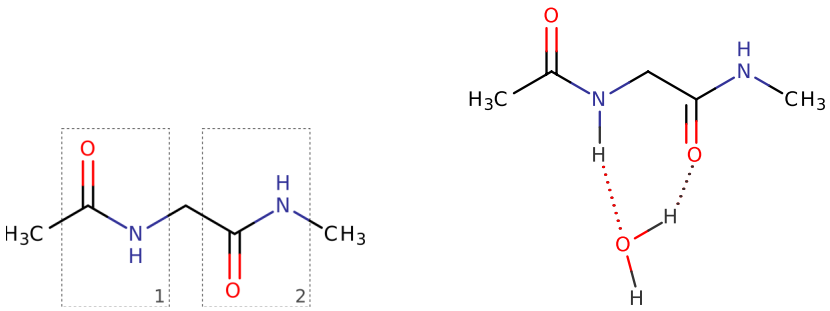

FIG. 3. The model dipeptide. (a) Convention used in the text to distinguish the peptide units. (b) Dipeptide monohydrate.

the individual peptide groups of uracil and the model dipeptide by the numbering presented in Figs. 2(a) and 3(a), respectively.

1. Geometries and excited state character

The geometries of all three uracil monohydrates were optimized analogous to Ref. 61. Following DeFusco's *et al.* choice for the active space, seven occupied orbitals (π_{CC} and π_{CO}, π_N, n_O for each peptide unit) and three unoccupied orbitals (π^*_{CC} and $2 \times \pi^*_{CO}$) were selected. As determined by the difference of charge densities (see Fig. S1 of the supplementary material),[67] a local transition in the carbonyl group from the oxygen lone pair to the π^*(CO) orbital constitutes the first (CO-1) and third (CO-2) excited states. The S_2 state involves mainly a transition from the nitrogen lone pair (N-2) to several π^* orbitals of the ring, whereas in the S_4 state, the transition originates from the other nitrogen lone pair (N-1). In both states, also the π orbital of the carbonyl group CO-2 takes part in the transition.

The equilibrium structure of the model dipeptide monohydrate was determined at the B3LYP/cc-pVTZ level of theory. As proposed by Serrano-Andrés and Fülscher, for both peptide units, the π_{CO}, π_N, n_O, and π^*_{CO} orbitals together with the corresponding six electrons have been included in the active space.[63] The lowest excited state is determined by a local transition from the lone pair oxygen to the π^* orbital of the carbonyl group (CO-1). The S_2 state involves the complementary transition of the second carbonyl group. In the S_4 and S_6 states, a local excitation from the nitrogen lone pair to the π^*(CO) orbital of the respective peptide group (S_4: 2, S_6: 1) is the dominating transition. The aforementioned charge transfer excitation was identified in two states. The S_3 state involves a transition from the nitrogen lone pair to the neighbouring carbonyl group (π_1(N) $\rightarrow \pi^*_2$(CO)). In the charge density difference plot, a smaller contribution from the π_1(CO) is also observed. In the S_5 state, π_1(N) is still involved, while the transition from the oxygen lone pair n_1(O) $\rightarrow \pi^*_2$(CO) makes up the main part.

The bromine monohydrate's geometry was optimized with second order Møller-Plesset perturbation theory (MP2) employing the aug-cc-pVDZ basis set. The active space for this system comprises seven occupied orbitals ($2 \times \sigma_g, \sigma_u$ and doubly degenerate π_u, π_g) and one unoccupied σ^*_u orbital. By defining the Br–Br bond as the z-axis and the x-axis to lie in the plane perpendicular to the molecular plane of H_2O, the first four excited states are characterized by $\pi_x \rightarrow \sigma^*_z$ (S_1, S_3) and $\pi_y \rightarrow \sigma^*_z$ (S_2, S_4) transitions. The S_5 state has double excitation character and involves both π_x and π_y orbitals. The respective cartesian coordinates of all tested systems are listed in the supplementary material (Tables S2-S6).[67] It should be mentioned that a comparison of excitation energies to experimental results was not the aim of this study. Neither the extent of the solvation shell nor the method is efficient enough to obtain comparable values. For that reason, we focus solely on the effect of the linearization of the non-additive functionals and non-orthogonality.

B. Conventional FDET calculations

The conventional FDET calculations were carried out primarily to set a standard to which the results from the *linearized FDET* calculations are compared. In order to quantify the extent of non-orthogonality, wave function overlaps $\langle \Psi^{sc}_I | \Psi^{sc}_J \rangle$ of self-consistent wave functions were computed. The corresponding table can be found in the mentary material (Table S1).[67] For all five systems, the wave function overlaps are in the range of 10^{-8} to 10^{-5}. There are only three exceptions where the values are actually one order of magnitude larger, namely, $\langle \Psi^{sc}_1 | \Psi^{sc}_3 \rangle$ (U3 conformer), $\langle \Psi^{sc}_2 | \Psi^{sc}_3 \rangle$ (dipeptide), and $\langle \Psi^{sc}_5 | \Psi^{sc}_6 \rangle$ (dipeptide). Wave function overlaps between the ground state of a system and its excited states $\langle \Psi^{sc}_0 | \Psi^{sc}_J \rangle$ are for all tested systems comparably small. Only one value of this group reaches 10^{-5} (case of U4). Comparable wave function overlap values were obtained in an embedded full CI calculation presented in Ref. 65. Analysis of the density difference between the self-consistent states shows that whenever a depletion of the density occurs close to hydrogen bonds, the wave function overlap increases.

We expect the non-orthogonality to become an issue worth considering for transition properties, for instance, oscillator strengths, although the only available work in the literature to this topic suggests only a small impact.[65]

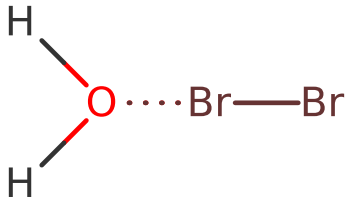

FIG. 4. Bromine monohydrate.

TABLE I. Difference between self-consistent and linearized total energies in electronvolts.

	U1	U3	U4	Dipeptide	Bromine
S_0	2.91×10^{-07}	1.41×10^{-07}	2.26×10^{-07}	4.27×10^{-07}	9.78×10^{-06}
S_1	-1.11×10^{-06}	1.45×10^{-03}	1.23×10^{-03}	4.27×10^{-06}	-1.96×10^{-04}
S_2	2.51×10^{-05}	1.52×10^{-06}	4.86×10^{-05}	9.68×10^{-04}	-1.98×10^{-04}
S_3	1.47×10^{-03}	8.55×10^{-06}	5.66×10^{-06}	8.35×10^{-05}	-2.11×10^{-04}
S_4	1.10×10^{-05}	1.32×10^{-05}	9.22×10^{-05}	-2.23×10^{-05}	-2.07×10^{-04}
S_5				7.72×10^{-05}	-1.21×10^{-05}
S_6				1.92×10^{-05}	

C. Linearized FDET calculations

The total energy in terms of linearized FDET was evaluated employing the ground state density of the isolated system ρ_A^{isol} as the reference density. The difference between the self-consistent total energies and the total energies obtained by linearization is collected in Table I. Concerning the uracil systems, the linearized total energies show very little deviation from the self-consistent total energies. Only for the states affected by the presence of the water molecule, this difference becomes

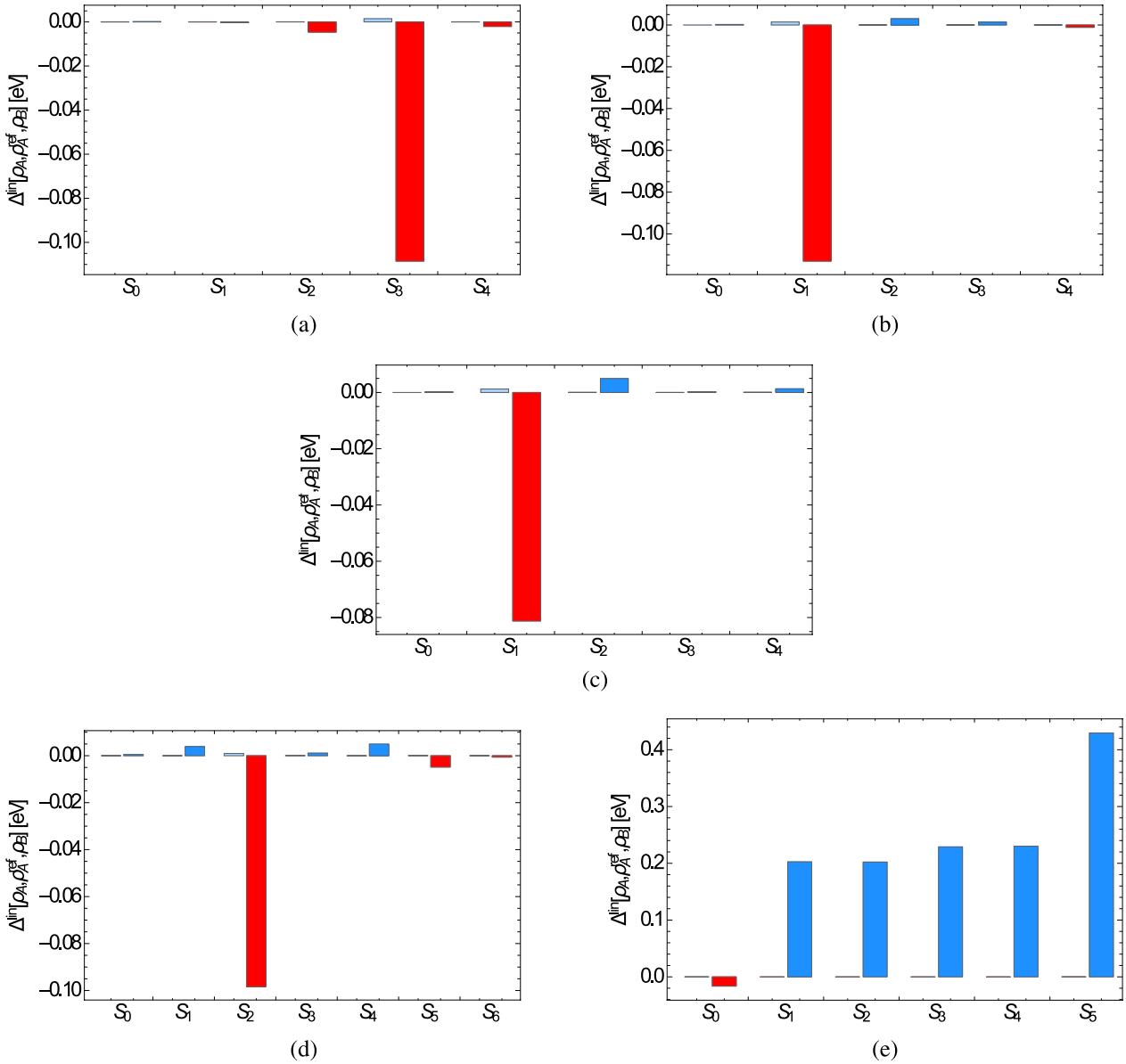

FIG. 5. Magnitude of $\Delta^{lin}[\rho_A, \rho_A^{ref}, \rho_B]$. For the sake of comparison, the respective values from Table I are also included as the first bar for each state. The second bar denotes $\Delta^{lin}[\rho_A, \rho_A^{ref}, \rho_B]$. A blue/red fill marks a positive/negative value. (a) Uracil — U1. (b) Uracil — U3. (c) Uracil — U4. (d) Dipeptide. (e) Bromine.

larger up to the amount of ca. 1 meV. The other two systems show a similar behaviour, whereas for bromine monohydrate, the differences are at least one order of magnitude smaller for the affected states (S_1–S_5). Another interesting trend is the consistently small magnitude of the differences for the ground states compared to excited states. Since both reference density and CASCI density are ground state densities in this case, the only difference between them is the effect of the embedding, i.e., these differences are predominantly determined by the electronic polarization of the embedded species by the environment. Among the tested systems, bromine monohydrate is the system in which the polarization of the ground state density is most apparent (compare Fig. 5). Here, $\Delta^{lin}[\rho_A, \rho_A^{ref}, \rho_B]$ of the ground state is approximately one fifth of maximal Δ^{lin} value in the four other monohydrates. Another way to put it is that the difference $\Delta\rho(\vec{r}) = \rho_A^I(\vec{r}) - \rho_A^{ref}(\vec{r})$ due to polarization is smaller than the difference due to excitation.

D. Numerical importance of $\Delta^{lin}[\rho_A, \rho_A^{ref}, \rho_B]$

Generally speaking, several factors determine the sign and magnitude of $\Delta^{lin}[\rho_A, \rho_A^{ref}, \rho_B]$. Its magnitude will decrease the more the difference $\rho_A^I(\vec{r}) - \rho_A^{ref}(\vec{r})$ is spatially separated of $\rho_B(\vec{r})$ since the nonelectrostatic part of the embedding potential depends strongly on the overlap of $\rho_A(\vec{r})$ and $\rho_B(\vec{r})$. Evidently this effect becomes most noticeable in systems where $\rho_B(\vec{r})$ is represented by a single molecule as it is the case in this study. In most cases, $\left.\frac{\delta E_{xct}^{nad}[\rho_A,\rho_B]}{\delta\rho_A(\vec{r})}\right|_{\rho_A=\rho_A^{ref}}$ is a repulsive potential in the extent of ρ_A.[39,66,28] As a consequence, the sign of $\Delta^{lin}[\rho_A, \rho_A^{ref}, \rho_B]$ is determined by the density difference. Depending on the location relative to $\rho_B(\vec{r})$, the positive and negative contributions to $\Delta^{lin}[\rho_A, \rho_A^{ref}, \rho_B]$ can cancel each other out to a certain extent.

Figure 5 shows the magnitude of $\Delta^{lin}[\rho_A, \rho_A^{ref}, \rho_B]$ for every computed state of the chosen model systems. Considering the uracil monohydrates first, $\Delta^{lin}[\rho_A, \rho_A^{ref}, \rho_B] \approx 0.1$ eV for the states which are affected by the presence of $\rho_B(\vec{r})$, while for all other states, this term becomes negligibly small (less than 0.01 eV). There are small variations in the extent of $\Delta^{lin}[\rho_A, \rho_A^{ref}, \rho_B]$ with regards to the three uracil systems, of which conformer U4 shows the smallest value. It is the same monohydrate which has also the longest hydrogen bond to the carbonyl oxygen compared to the other two (1.93 Å vs. 1.90 Å).

As for the dipeptide, $\Delta^{lin}[\rho_A, \rho_A^{ref}, \rho_B]$ is noticeably large only in the case of S_2, the local $n_2(\mathrm{O}) \rightarrow \pi_2^*(\mathrm{CO})$ transition, and almost the same value compared to the uracil monohydrates. As for the charge transfer states S_3 and S_5, $\Delta^{lin}[\rho_A, \rho_A^{ref}, \rho_B]$ comprises only 1% and 5% of the value in S_2. Although the excitation involves the same carbonyl group as in S_2, the increase of the density is spread over the whole peptide group (CON-1). Since the charge-transfer excitation in S_5 involves the oxygen lone pair on carbonyl group CO-1, we expect $\Delta^{lin}[\rho_A, \rho_A^{ref}, \rho_B]$ to be similarly large as in the case of S_2, if the water molecule was hydrogen bonded to CO-1 instead of CO-2. Finally, for the bromine monohydrate, $\Delta^{lin}[\rho_A, \rho_A^{ref}, \rho_B]$ exceeds 0.1 eV for every excited state. In fact, it reaches 0.2 eV for the first four excited states and 0.4 eV in the case of S_5. Also the ground state involves a larger value of approximately 0.02 eV compared to the other tested systems, where it is two orders of magnitude smaller. The fact that $\Delta^{lin}[\rho_A, \rho_A^{ref}, \rho_B]$ varies strongly depending on the character of the state and the proximity of ρ_B, while the difference between self-consistent and linearized total energy is very small, gives linearized FDET a great robustness. Regarding the implementation, $\Delta^{lin}[\rho_A, \rho_A^{ref}, \rho_B]$ is evaluated once the reference density ρ_A^{ref}, the density of the respective state ρ_A^I, and the nonelectrostatic part of the fixed embedding potential $\left.\frac{\delta E_{xct}^{nad}[\rho_A,\rho_B]}{\delta\rho_A(\vec{r})}\right|_{\rho_A=\rho_A^{ref}}$ are available. This *a posteriori* analysis makes linearized FDET ideal for perturbational methods. Furthermore, the magnitude of $\Delta^{lin}[\rho_A, \rho_A^{ref}, \rho_B]$ can be used as an analysis tool to determine the quality of the chosen reference density.

VI. DISCUSSIONS AND CONCLUSIONS

Embedded wave functions obtained in FDET can be associated with different electronic states. Unfortunately, due to ρ_A-dependency of the non-electrostatic components of the FDET embedding potential, they are not mutually orthogonal. The *linearized FDET* framework assures both the self-consistency between the energy and the embedded wave function and the orthogonality of embedded wave functions. It is shown that practically the same results (agreement of the excitation energies within 10^{-3} eV or less) are obtained using a linearized approximation for the non-electrostatic components of the functional for the FDET embedding potential. Assuring orthogonality of the stationary states obtained in FDET brings significant advantages.

- *Reduction of the computational costs*. The many-electron problem (Eq. (8)) has to be solved only once (see Fig. 1).
- *Reduction of the imbalance of errors in the energy of different states*. In conventional FDET calculations, the error in the energy is determined by two factors: the error in the used approximated functional for $E_{xct}^{nad}[\rho_A, \rho_B]$ and the error in the corresponding potential ($\frac{\delta E_{xct}^{nad}[\rho_A,\rho_B]}{\delta\rho_A(\vec{r})}$). The errors in the embedding potential might be different if evaluated at different ρ_A. In *linearized FDET*, on the other hand, the embedding potential is the same for all electronic states of the embedded species.
- *Orthogonality of embedded wave functions for different states*. It is assured by construction owing to the common embedding potential.

The numerical results show also that the *linearized FDET* is a robust procedure. Despite the fact that the magnitude of $\Delta^{lin}[\rho_A, \rho_A^{ref}, \rho_B]$ is not constant and non-negligible in many cases (the maximal value in this study is 0.43 eV), the excitation energies from conventional and linearized FDET are practically indistinguishable for the chosen reference density $\rho_A^{ref}(\vec{r})$, which was the ground-state density of the isolated chromophore. The stationary FDET densities $\rho_A^I(\vec{r})$ differ from $\rho_A^{ref}(\vec{r})$ due to the polarization of the chromophore by the environment and due to the excitation. Numerical results show that linearization of $\tilde{E}_{xct}^{nad}[\rho_A, \rho_B]$ provides an adequate treatment

of the two effects. The former one is nevertheless numerically less significant.

Concerning the numerical importance of $\Delta^{lin}[\rho_A, \rho_A^{ref}, \rho_B]$, which can be used as the detector of the importance of non-linearity in a given electronic state of the embedded species, we notice that cases where it is negligible can be identified prior to the calculations. It can be expected to be small if the domain in real space where the electron density changes upon excitation do not overlap significantly with $\rho_B(\vec{r})$. In such a case, the electrostatic component of the embedding potential dominates. Since this component is ρ_A-independent, the non-orthogonality of embedded wave functions does not occur (zero overlap case) or can be neglected. It is important to notice that the evaluation of $\Delta^{lin}[\rho_A, \rho_A^{ref}, \rho_B]$ involves negligible additional numerical cost as it consists of one numerical integration over a grid in R^3.

The numerical examples and all the considerations of the present work concerned variational methods to solve Eq. (8). Linearized FDET expressions for the energy and the embedding potential can be applied in a straightforward manner, also in combination with perturbation theory or coupled-cluster type of methods of quantum chemistry used to solve Eq. (17). In such a case, the embedding potential in Eq. (8) is also ρ_A-independent and $\Delta^{lin}[\rho_A, \rho_A^{ref}, \rho_B]$ involves integration of the embedding potential with the difference between the reference density and the density obtained in perturbational calculations. The Hartree-Fock density should be used as $\rho_A^{ref}(\vec{r})$ and the MP2 density should be used as ρ_A in Eqs. (16) and (19), for instance.

Finally, the numerical examples concern a particular approximation for $E_{xct}^{nad}[\rho_A, \rho_B]$. It can be applied without any modification for other approximations for this functional.

Several researchers developed methods in which at certain stage, Eq. (13) is solved in a simplified manner consisting of using some fixed density (for example, the ground state density $\rho_A^0(\vec{r})$[12,40,23,11,16]) in the evaluation of the embedding potential instead of the actual density $\rho_A^I(\vec{r})$. To evaluate the total energy, the functional given in Eq. (14) is used. In such a case, different stationary states are obviously orthogonal but this leads to inconsistent energy and wave function. Self-consistency can easily be restored by means of using Eq. (19) instead of Eq. (14). To this end, it is enough to use as $\rho_A^{ref}(\vec{r})$ in Eq. (19) the density $\rho_A^0(\vec{r})$ for which the fixed embedding potential was evaluated. The numerical difference between the energies obtained using the two equations is due to quadratic and higher contributions.

ACKNOWLEDGMENTS

This research was supported by grants from Swiss National Science Foundation (Grant No. 200021_152779). F.A. gratefully acknowledges support from the FIRB "PROGRAMMA FUTURO IN RICERCA" RBFR1248UI by the Italian "Ministero dell'Istruzione, dell'Università e della Ricerca" (MIUR).

[1]T. A. Wesolowski and A. Warshel, "Frozen density functional approach for *ab initio* calculations of solvated molecules," J. Phys. Chem. **97**(30), 8050–8053 (1993).
[2]T. A. Wesolowski, "Embedding a multideterminantal wave function in an orbital-free environment," Phys. Rev. A **77**, 012504 (2008).
[3]K. Pernal and T. A. Wesolowski, "Orbital-free effective embedding potential: Density-matrix functional theory case," Int. J. Quantum Chem. **109**, 2520–2525 (2009).
[4]J. P. Perdew and M. Levy, "Extrema of the density functional for the energy—Excited-states from the ground-state theory," Phys. Rev. B **31**(10), 6264–6272 (1985).
[5]Y. G. Khait and M. R. Hoffmann, "Embedding theory for excited states," J. Chem. Phys. **133**(4), 044107 (2010).
[6]T. A. Wesolowski, "Hydrogen-bonding-induced shifts of the excitation energies in nucleic acid bases: An interplay between electrostatic and electron density overlap effects," J. Am. Chem. Soc. **126**(37), 11444–11445 (2004).
[7]T. A. Wesolowski, "Embedding potentials for excited states of embedded species," J. Chem. Phys. **140**(18), 18A530 (2014).
[8]L. I. Bendavid and E. A. Carter, *Status in Calculating Electronic Excited States in Transition Metal Oxides from First Principles* (Springer, 2014).
[9]T. A. Wesolowski, S. Shedge, and X. Zhou, "Frozen-density embedding strategy for multilevel simulations of electronic structure," Chem. Rev. **115**(12), 5891 (2015).
[10]C. Daday, C. König, J. Neugebauer, and C. Filippi, "Wavefunction in density functional theory embedding for excited states: Which wavefunctions, which densities?," ChemPhysChem **15**, 3205–3217 (2014).
[11]C. Daday, C. König, O. Valsson, J. Neugebauer, and C. Filippi, "State-specific embedding potentials for excitation-energy calculations," J. Chem. Theory Comput. **9**(5), 2355–2367 (2013).
[12]A. S. P. Gomes, C. R. Jacob, and L. Visscher, "Calculation of local excitations in large systems by embedding wave-function theory in density-functional theory," Phys. Chem. Chem. Phys. **10**(35), 5353–5362 (2008).
[13]S. Höfener, "Coupled-cluster frozen-density embedding using resolution of the identity methods," J. Comput. Chem. **35**(23), 1716–1724 (2014).
[14]O. Roncero, A. Aguado, F. A. Batista-Romero, M. I. Bernal-Uruchurtu, and R. Hernández-Lamoneda, "Density-difference-driven optimized embedding potential method to study the spectroscopy of Br_2 in water clusters," J. Chem. Theory Comput. **11**, 1155–1164 (2015).
[15]D. Lahav and T. Kluner, "A self-consistent density based embedding scheme applied to the adsorption of CO on Pd(111)," J. Phys.: Condens. Matter **19**, 226001 (2007).
[16]T. Dresselhaus, J. Neugebauer, S. Knecht, S. Keller, Y. Ma, and M. Reiher, "Self-consistent embedding of density-matrix renormalization group wavefunctions in a density functional environment," J. Chem. Phys. **142**, 044111 (2014).
[17]N. Govind, Y. A. Wang, A. J. R. da Silva, and E. A. Carter, "Accurate *ab initio* energetics of extended systems via explicit correlation embedded in a density functional environment," Chem. Phys. Lett. **295**, 129–134 (1998).
[18]N. Govind, Y. A. Wang, and E. A. Carter, "Electronic-structure calculations by first-principles density-based embedding of explicitly correlated systems," J. Chem. Phys. **110**(16), 7677–7688 (1999).
[19]M. Svensson, S. Humbel, R. D. J. Froese, T. Matsubara, S. Sieber, and K. Morokuma, "Oniom: A multilayered integrated MO+MM method for geometry optimizations and single point energy predictions. A test for diels-alder reactions and $Pt(P(t-Bu)_3)_2 + h_2$ oxidative addition," J. Phys. Chem. **100**(50), 19357–19363 (1996).
[20]T. A. Wesolowski, "One-electron equations for embedded electron density: Challenge for theory and practical payoffs in multi-level modelling of soft condensed matter," in *Computational Chemistry: Reviews of Current Trends* (World Scientific, 2006), Vol. X, pp. 1–82.
[21]J. Neugebauer, "Chromophore-specific theoretical spectroscopy: From subsystem density functional theory to mode-specific vibrational spectroscopy," Phys. Rep. **489**(1–3), 1–87 (2010).
[22]C. R. Jacob and J. Neugebauer, "Subsystem density-functional theory," Wiley Interdiscip. Rev.: Comput. Mol. Sci. **4**(4), 325–362 (2014).
[23]S. Höfener, A. S. P. Gomes, and L. Visscher, "Solvatochromic shifts from coupled-cluster theory embedded in density functional theory," J. Chem. Phys. **139**(10), 104106 (2013).
[24]T. Helgaker, J. Olsen, and P. Jorgensen, *Molecular Electronic-Structure Theory* (Wiley, 2013).
[25]B. J. Zhou, Y. A. Wang, and E. A. Carter, "Transferable local pseudopotentials derived via inversion of the Kohn-Sham equations in a bulk environment," Phys. Rev. B **69**(12), 125109 (2004).
[26]O. Roncero, M. P. de Lara-Castells, P. Villarreal, F. Flores, J. Ortega, M. Paniagua, and A. Aguado, "An inversion technique for the calculation of embedding potentials," J. Chem. Phys. **129**(18), 184104 (2008).
[27]J. D. Goodpaster, N. Ananth, F. R. Manby, and T. F. Miller III, "Exact nonadditive kinetic potentials for embedded density functional theory," J. Chem. Phys. **133**(8), 084103 (2010).

[28]S. Fux, C. R. Jacob, J. Neugebauer, L. Visscher, and M. Reiher, "Accurate frozen-density embedding potentials as a first step towards a subsystem description of covalent bonds," J. Chem. Phys. **132**(16), 164101 (2010).
[29]J.-D. Chai and J. D. Weeks, "Orbital-free density functional theory: Kinetic potentials and *ab initio* local pseudopotentials," Phys. Rev. B **75**, 205122 (2007).
[30]D. G Artiukhin, C. R. Jacob, and J. Neugebauer, "Excitation energies from frozen-density embedding with accurate embedding potentials," J. Chem. Phys. **142**, 234101 (2015).
[31]M. Dulak, J. W. Kaminski, and T. A. Wesolowski, "Linearized orbital-free embedding potential in self-consistent calculations," Int. J. Quantum Chem. **109**(9), 1886–1897 (2009).
[32]B. Mennucci and J. Tomasi, "Continuum solvation models: A new approach to the problem of solute's charge distribution and cavity boundaries," J. Chem. Phys. **106**(12), 5151–5158 (1997).
[33]A. Klamt and G. Schüürmann, "Cosmo: A new approach to dielectric screening in solvents with explicit expressions for the screening energy and its gradient," J. Chem. Soc., Perkin Trans. 2 **2**(5), 799–805 (1993).
[34]T. D. Poulsen, P. R. Ogilby, and K. V. Mikkelsen, "Linear response properties for solvated molecules described by a combined multiconfigurational self-consistent-field/molecular mechanics model," J. Chem. Phys. **116**(9), 3730–3738 (2002).
[35]L. Jensen, P. Th. van Duijnen, and J. G. Snijders, "A discrete solvent reaction field model within density functional theory," J. Chem. Phys. **118**(2), 514–521 (2003).
[36]J. Kongsted, A. Osted, K. V. Mikkelsen, and O. Christiansen, "Linear response functions for coupled cluster/molecular mechanics including polarization interactions," J. Chem. Phys. **118**(4), 1620–1633 (2003).
[37]M. Humbert-Droz, X. Zhou, S. V. Shedge, and T. A. Wesolowski, "How to choose the frozen density in frozen-density embedding theory-based numerical simulations of local excitations?," Theor. Chem. Acc. **133**(1), 1–20 (2014).
[38]A. Savin and T. A. Wesolowski, "Orbital-free embedding effective potential in analytically solvable cases," Prog. Theor. Chem. Phys. **19**, 327–339 (2009).
[39]P. de Silva and T. A. Wesolowski, "Exact non-additive kinetic potentials in realistic chemical systems," J. Chem. Phys. **137**(9), 094110 (2012).
[40]D. K. Kanan, S. Sharifzadeh, and E. A. Carter, "Quantum mechanical modeling of electronic excitations in metal oxides: Magnesia as a prototype," Chem. Phys. Lett. **519**, 18–24 (2012).
[41]M. Levy and J. P. Perdew, "The constrained search formulation of density functional theory," in *Density Functional Methods In Physics*, NATO ASI Series B Vol. 123 (Springer, 1985), pp. 11–30.
[42]W. Kohn and L. J. Sham, "Self-consistent equations including exchange and correlation effects," Phys. Rev. **140**(4A), A1133–A1138 (1965).
[43]E. H. Lieb, "Density functionals for coulomb-systems," Int. J. Quantum Chem. **24**(3), 243–277 (1983).
[44]A. Szabo and N. S. Ostlund, *Modern Quantum Chemistry. Introduction to Advanced Electronic Structure Theory* (McGraw-Hill, 1982).
[45]F. Aquilante and T. A. Wesolowski, "Self-consistency in frozen-density embedding theory based calculations," J. Chem. Phys. **135**(8), 084120 (2011).
[46]M. E. Casida, "Time-dependent density-functional response theory for molecules," in *Recent Advances in Computational Chemistry* edited by D. P. Chong (World Scientific, Singapore, 1995), Vol. 1. Pt. 1, p. 155.
[47]J. M. Garcia Lastra, J. W. Kaminski, and T. A. Wesolowski, "Orbital-free effective embedding potential at nuclear cusps," J. Chem. Phys. **129**, 074107 (2008).
[48]F. Aquilante, L. de Vico, N. Ferré, G. Ghigo, P.-Å. Malmqvist, P. Neogrády, T. B. Pedersen, M. Pitoňák, M. Reiher, B. O. Roos, L. Serrano-Andrés, M. Urban, V. Veryazov, and R. Lindh, "MOLCAS 7: The next generation," J. Comput. Chem. **31**(1), 224–247 (2010).
[49]F. Aquilante, T. B. Pedersen, V. Veryazov, and R. Lindh, Wiley Interdiscip. Rev.: Comput. Mol. Sci. **3**, 143 (2013).
[50]T. H. Dunning, Jr., "Gaussian basis sets for use in correlated molecular calculations. I. The atoms boron through neon and hydrogen," J. Chem. Phys. **90**, 1007 (1989).
[51]D. E. Woon and T. H. Dunning, Jr., "Gaussian basis sets for use in correlated molecular calculations. III. The atoms aluminium through argon," J. Chem. Phys. **98**, 1358 (1993).
[52]F. Aquilante, L. Boman, J. Boström, H. Koch, T. B. Pedersen, A. Sanchez de Merás, and R. Lindh, "Cholesky decomposition techniques in electronic structure theory," in *Challenges and Advances in Computational Chemistry and Physics*, edited by M. G. Papadopoulos, R. Zalesny, P. G. Mezey, and J. Leszczynski (Springer, 2011), Vol. 13, pp. 301–344.
[53]J. Boström, M. Pitonak, F. Aquilante, P. Neogrady, T. B. Pedersen, and R. Lindh, "Coupled cluster and møller–plesset perturbation theory calculations of noncovalent intermolecular interactions using density fitting with auxiliary basis sets from cholesky decompositions," J. Chem. Theory Comput. **8**(6), 1921–1928 (2012).
[54]J. Boström, M. G. Delcey, F. Aquilante, L. Serrano-Andres, T. B. Pedersen, and R. Lindh, "Calibration of cholesky auxiliary basis sets for multiconfigurational perturbation theory calculations of excitation energies," J. Chem. Theory Comput. **6**, 747–754 (2010).
[55]M. G. Delcey, L. Freitag, T. B. Pedersen, F. Aquilante, R. Lindh, and L. Gonzalez, "Analytical gradients of complete active space self-consistent field energies using cholesky decomposition: Geometry optimization and spin-state energetics of a ruthenium nitrosyl complex," J. Chem. Phys. **140**(17), 174103 (2014).
[56]J. Boström, V. Veryazov, F. Aquilante, T. B. Pedersen, and R. Lindh, "Analytical gradients of the second-order Møller–Plesset energy using cholesky decompositions," Int. J. Quantum Chem. **114**(5), 321–327 (2014).
[57]J. Boström, F. Aquilante, T. B. Pedersen, and R. Lindh, "Analytical gradients of Hartree–Fock exchange with density fitting approximations," J. Chem. Theory Comput. **9**(1), 204–212 (2012).
[58]L. H. Thomas, "The calculation of atomic fields," Math. Proc. Cambridge Philos. Soc. **23**, 542 (1927).
[59]E. Fermi, "Un metodo statistico per la determinazione de alcune prioprietà dell'atomo," Rend. Accad. Naz. Lincei **6**, 602 (1927).
[60]J. P. Perdew, M. Ernzerhof, and K. Burke, "Rationale for mixing exact exchange with density functional approximations," J. Chem. Phys. **105**, 9982 (1996).
[61]A. DeFusco, J. Ivanic, M. W. Schmidt, and M. S. Gordon, "Solvent-induced shifts in electronic spectra of uracil," J. Phys. Chem. A **115**(18), 4574–4582 (2011).
[62]M. J. G. Peach, P. Benfield, T. Helgaker, and D. J. Tozer, "Excitation energies in density functional theory: An evaluation and a diagnostic test," J. Chem. Phys. **128**, 044118 (2008).
[63]L. Serrano-Andrés and M. P. Fülscher, "Theoretical study of the electronic spectroscopy of peptides. III. Charge-transfer transitions in polypeptides," J. Am. Chem. Soc. **120**(42), 10912–10920 (1998).
[64]M. I. Bernal-Uruchurtu, R. Hernández-Lamoneda, and K. C. Janda, "On the unusual properties of halogen bonds: A detailed *ab initio* study of X_2-$(H_2O)_{1-5}$ clusters (X = Cl and Br)," J. Phys. Chem. A **113**(19), 5496–5505 (2009).
[65]T. Dresselhaus and J. Neugebauer, "Part and whole in wavefunction/DFT embedding," Theor. Chem. Acc. **134**(8), 1–15 (2015).
[66]M. Dulak, R. Kevorkyants, F. Tran, and T. A. Wesolowski, "One-electron equations for embedded electron density and their applications to study electronic structure of atoms and molecules in condensed phase," Chimia **59**(7-8), 488–492 (2005).
[67]See supplementary material at http://dx.doi.org/10.1063/1.4933372 for Cartesian coordinates of all systems used in the present work, wave function overlap integrals and density differences of self-consistent ground state and other self-consistent states of each system.